On-Chip Diffraction-Free Beam Guiding beyond the Light Cone

Ye Lin,[1] Tianhua Feng,[1] Sheng Lan,[2] Jin Liu,[3] and Yi Xu[1,*]

[1] *Department of Electronic Engineering, College of Information Science and Technology, Jinan University, Guangzhou 510632, China*

[2] *School of Information and Optoelectronic Science and Engineering, South China Normal University, Guangzhou 510006, China*

[3] *State Key Laboratory of Optoelectronic Materials and Technologies, School of Physics, Sun Yat-sen University, Guangzhou 510275, China*

(Received 19 December 2019; revised manuscript received 29 March 2020; accepted 28 April 2020; published 12 June 2020)

On-chip channelless diffraction-free beam guiding enables dense integration of optical circuits in a reconfigurable manner, where total internal reflection, which is considered the cornerstone of guided-wave optics, is utilized to confine light in the out-of-plane direction. Here, we theoretically propose a physical mechanism to achieve on-chip channelless diffraction-free beam guiding beyond the light cone, utilizing the physics of bound states in the continuum. A bound state in the continuum with a tailored spatial dispersion plays an important role in cancelling both the in-plane diffraction and the out-of-plane scattering when the condition for total internal reflection is not satisfied. As a proof-of-concept verification, we experimentally demonstrate such an effect based on an all-dielectric platform using microwaves. The on-chip channelless diffraction-free beam guiding beyond the light cone also allows direct free-space coupling to such self-collimation modes. Our results may open up an avenue for exploring the physics and applications of guided-wave optics.

DOI: 10.1103/PhysRevApplied.13.064032

I. INTRODUCTION

Diffraction is a universal property of light that imposes an ultimate limitation on free-space optical communication [1]. As a result, the management of diffraction in optics is crucial from the point of view of both fundamental science and applications [2–5]. Great efforts have been made to manage the diffraction of light by utilizing artificial structures, such as photonic lattices and photonic crystals [6–20]. Based on Lieb photonic lattices, a completely flat band can be achieved along the direction perpendicular to the lattice period [21]. Although diffraction can also be cancelled by optical nonlinearity, manifested as optical spatial solitons [4], diffraction-free beam guiding within the scope of linear optics is very important for realizing low-power on-chip all-optical processing [2,5]. The so-called self-collimation (SC) phenomenon, originating from the nonlocal response of photonic-crystal (PhC) slabs, offers a unique solution for suppressing in-plane diffraction without an in-plane physical boundary (or a fixed optical axis) [9–12], facilitating the dense spatial multiplexing of optical signals [2]. In particular, the demonstration of macroscopic SC paves the way to realizing chip-scale all-optical logic components [13,15,19]. To date, all demonstrations of on-chip SC have relied strictly on total internal reflection (TIR) to guide light in the out-of-plane direction [2,6–13,15–20]; this is regarded as the cornerstone of guided-wave optics and is essentially below the light cone of the surrounding materials [1]. According to optical-waveguide theory, there is a fundamental cutoff frequency for an optical waveguide of a specified thickness, which is essentially imposed by the light cone of the surrounding materials [1]. Therefore, there is a general quest to break this limit and explore the possibility of diffraction-free beam guiding beyond the light cone.

Recently, the physics of bound states in the continuum (BICs), which were originally proposed in quantum mechanics [22], has attracted a large amount of research effort because of their counterintuitive nature [23], topological robustness to disorder effects [24,25], generality in physical systems [26–29], and potential applications in many disciplines [30]. Such embedded states can be regarded as localized wave solutions whose eigenfrequencies are real numbers, and fall inside a radiative continuum of extended states [30]. Particularly, optical BICs [24,25,31–69], especially BICs in flat optics, resemble ideal platforms for obtaining fruitful physics results and developing promising applications [24,25,31,32,36–39,41–43,45,47–62]. In such scenarios, BICs reside in the continuum beyond the light cone of the surrounding materials

*yi.xu@osamember.org

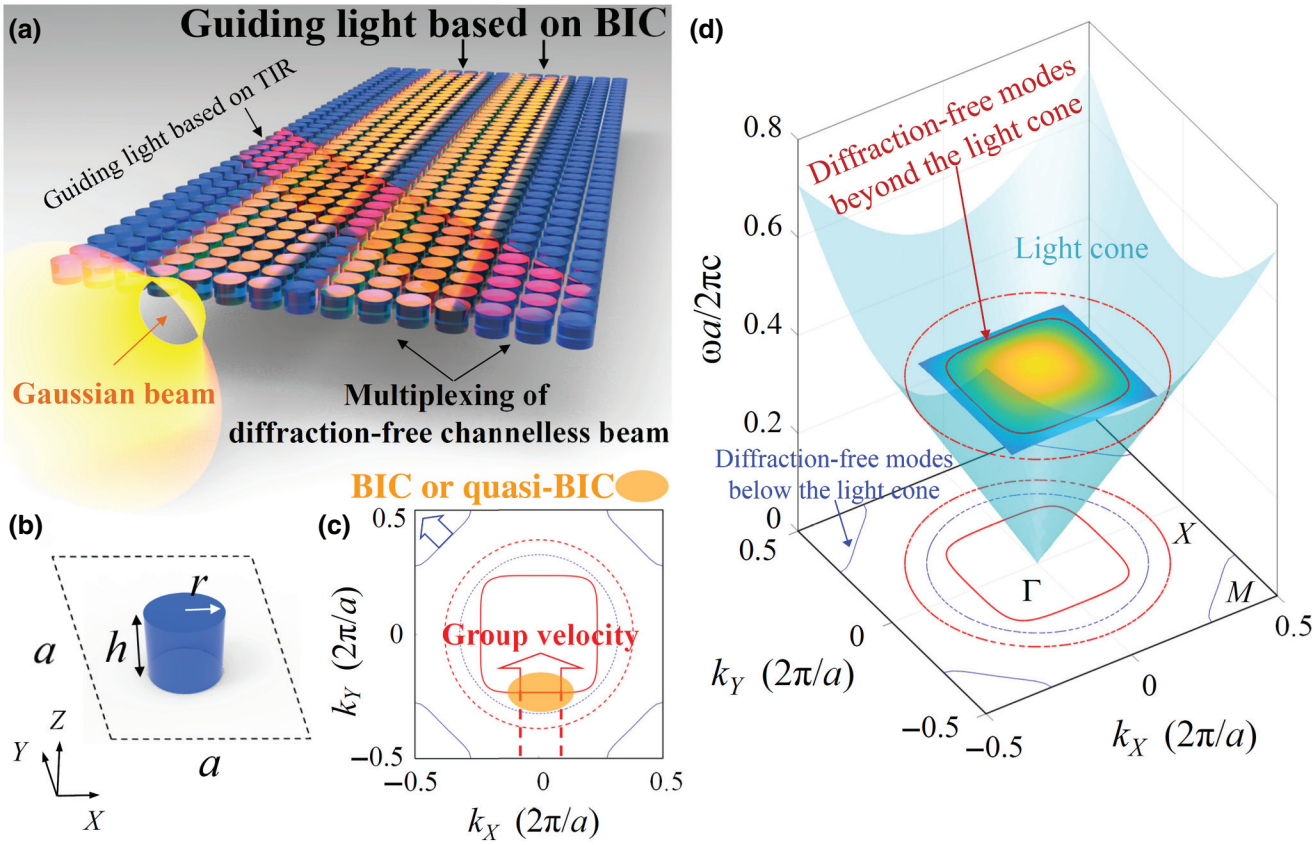

FIG. 1. (a) Schematic illustration of on-chip multiplexing of diffraction-free beams beyond and below the light cone of the surrounding material. Focused Gaussian beams are used to excite diffraction-free modes (in the Γ-X direction) beyond the light cone (orange). One of the diffraction-free modes (in the Γ-M direction) below the light cone is indicated in red. (b) Photonic-crystal slab formed from dielectric pillars ($\varepsilon = 9.6$) arranged in a square lattice with a lattice constant a. The radius r and height h are $0.442a$ and $0.608a$, respectively. (c),(d) General concept of nondiffractive beam guiding beyond the light cone. The color-coded surface in (d) indicates the band of the PhC slab, which features a square EFC (solid red lines) beyond the light cone (light blue surface), while there are also flat EFCs (solid blue lines) below the light cone at the corners of the FBZ. The corresponding EFCs of the surrounding materials are indicated by dashed circles. The guiding mechanism along the surface normal of the PhC slab for the diffraction-free modes beyond the light cone is enabled by the physics of BICs and quasi-BICs shown in (c), while the conventional mechanism for modes below the light cone is enabled by total internal reflection. The large arrows indicate the directions of the group velocity for the diffraction-free modes. The orange ellipse shows one of the four BICs and the related quasi-BIC region in the FBZ.

[30]. Symmetry-protected BICs are momentumless Bloch modes at the center of the Brillouin zone [36], while accidental BIC modes can exist away from the center of the Brillouin zone, which indicates the possibility of guiding light beyond the light cone [37,38,41,62–69]. However, such a beam-guiding effect based on a BIC either suffers from in-plane diffraction [37,41,62,68] or relies on an inevitable optical axis [38,63–67,69], limiting the applications of BICs in guiding diffraction-free light in a similar way to its counterpart below the light cone.

In this paper, we theoretically propose a mechanism to realize on-chip channelless diffraction-free beam guiding beyond the light cone, enabled by the physics of BICs and spatial dispersion simultaneously. The promising functionality of the proposed guiding mechanism is its ability to be compatible with diffraction-free beam guiding below the light cone at the same time, facilitating dense multiplexing of optical signals on the scale of a chip. We further provide an experimental demonstration using microwaves, which validates the generality of the proposed diffraction-free wave-guiding mechanism.

II. PHYSICAL MECHANISM OF DIFFRACTION-FREE BEAM GUIDING BEYOND THE LIGHT CONE

The vision of our idea is shown schematically in Fig. 1(a), where polychromatic diffraction-free beams are multiplexed based on a PhC slab in a channelless manner. Diffraction-free beams beyond(orange) and below (red) the light cone are guided by BICs and TIR, respectively. The PhC slab is formed simply from dielectric pillars of radius

r and thickness h arranged in a square lattice with a lattice constant a, as shown in Fig. 1(b). The physical mechanism regarding this concept is summarized in Figs. 1(c) and 1(d), where equifrequency contours (EFCs) for these two types of SC mode are shown in the first Brillouin zone (FBZ). Substantially differently from the SC mode (blue solid lines) below the light cone (the blue dashed circle), a square EFC exists beyond the light cone [see the red solid line superimposed on the band surface in Fig. 1(d)], which is confirmed by the EFCs projected into the first Brillouin zone. The corresponding EFCs of the surrounding materials are also shown by dashed circles. It should be pointed out that such square EFCs can be designed in a sophisticated way to be below the light cone [9,11], as guiding by TIR was once considered a canonical way to confine light perpendicular to a PhC slab. The physical mechanism of diffraction-free beam guiding based on a BIC is schematically shown in Fig. 1(c), where a single-resonance BIC and quasi-BIC modes are simultaneously allowed by spatial dispersion to cancel the in-plane diffraction. At the same time, out-of-plane leakage is prohibited or reduced by the BIC and quasi-BIC modes, where the radiative Q factors of these modes are substantially larger than the nonradiative Q factors limited by the effect of intrinsic disorder in fabrication [24,61]. As a result, this guiding mechanism can be regarded as a quasiguiding effect enabled by synchronous manipulation of the real (spatial dispersion) and imaginary (quasi-BICs with momentum) parts of the eigenfrequencies of the PhC slab.

In order to provide a quantitative picture of diffraction-free beam guiding beyond the light cone, we calculate the dispersion of the SC band beyond the light cone for a typical all-dielectric PhC slab; details of the PhC slab can be found in the caption of Fig. 1. We consider a symmetric case first, where the surrounding material is air. The effect of the substrate is addressed later. The band structures above the light cone are calculated by the finite-element method (FEM) (High Frequency Structure Simulator by Ansoft), where the eigenvalues of the source-free Maxwell equations in a given frequency range are evaluated for the PhC. Periodic boundary conditions are applied normal to the $\pm X$ and $\pm Y$ directions, while perfectly matched layer boundary conditions are used in the $\pm Z$ direction. The property of spatial dispersion can be also designed and evaluated by use of the semianalytical coupled-wave-theory framework [70], the mode-expansion method [71], and spatial-dispersion theory [72]. The underlying physics of the on-chip diffraction-free beam guiding beyond the light cone is based on the unique properties of single-resonance BICs, which rely on parameter tuning [37]. As a result, the conditions for such a BIC are quite sensitive to the parameters of the structure, which means that it can be effectively tuned by varying the lattice constant. According to the calculated dispersion along the Γ-X direction and the corresponding Q factors for small changes of the lattice

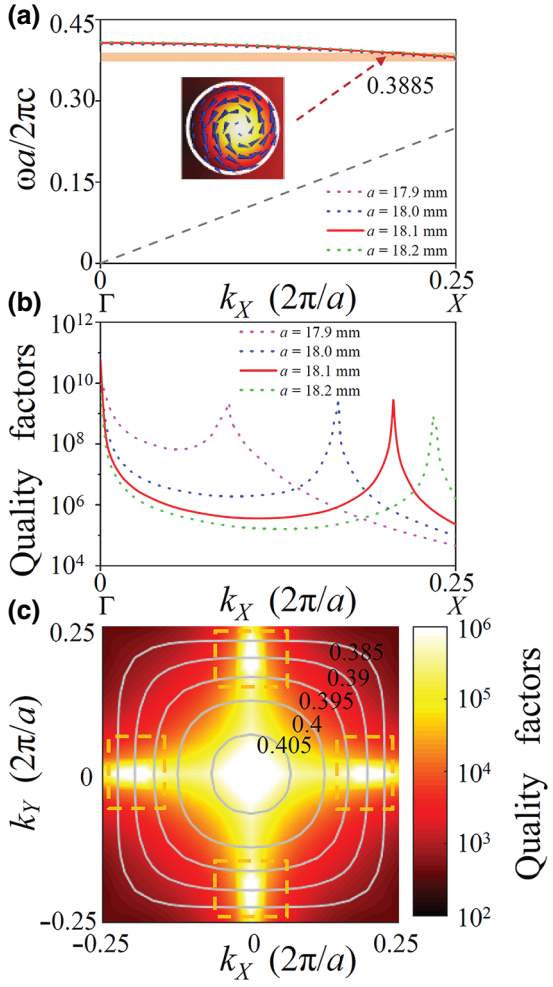

FIG. 2. (a) Dispersion properties along the Γ-X direction, where the results for four typical lattice constants, indicated in the inset, are shown. The light line (dashed gray line) is also shown. The bandwidth of the diffraction-free beam guiding (including quasiguiding) is outlined by the orange region. The electromagnetic distribution of a SC eigenmode in a unit cell is also presented, where the arrows indicate the electric field vectors and the color code shows the intensity of the magnetic field. (b) Corresponding Q factors of the modes shown in (a). (c) EFCs (solid gray lines) and distribution (superimposed) of Q factors in the FBZ. The color code represents the magnitude of the Q factors for the different modes. The dashed rectangles outline the regions where one can achieve diffraction-free beam guiding (or quasiguiding) beyond the light cone.

constant, shown in Figs. 2(a) and 2(b), the corresponding k vector of the single-resonance BIC with the imaginary part of the eigenfrequency minimized can be effectively tuned by varying the lattice constant a [see Fig. 2(b)], while the properties of the modal dispersion (corresponding to the real part of the eigenfrequency) are hardly affected [see Fig. 2(a)]. Therefore, one can match the single-resonance BIC condition with the targeted diffraction-free dispersion to realize diffraction-free beam guiding beyond the light cone.

The EFCs (solid gray lines) at several typical normalized frequencies and the corresponding Q factors (color coded) are shown superimposed on the FBZ in Fig. 2(c). There are four regions (shown by dashed rectangles) within the FBZ corresponding to on-chip diffraction-free beam guiding beyond the light cone. Such modes are SC modes whose EFCs are flat because of spatial dispersion, and they are quasi-BIC modes possessing sufficiently high Q factors (larger than 10^6) to reduce the out-of-plane radiation loss in a finite structure. The corresponding frequency range (orange) of these robust SC modes in the band diagram is shown in Fig. 2(a). As we can see from this figure, the SC region is substantially beyond the light cone, with k vectors centered at $0.2056 \times 2\pi/a$, and the guiding mechanism is fundamentally different from that in the state-of-the-art cases below the light cone [2,6–20]. It should be mentioned here that the concept of the light cone with respect to on-chip beam guiding needs to be handled carefully, especially for multilayer wave-guiding systems [73]. Furthermore, because the single-resonance BIC at $k_x = 0.2056 \times 2\pi/a$ along the Γ-X direction and the symmetry-protected BIC at the center of the Brillouin zone are close together in the FBZ, the Q factors of the Bloch modes within this range are all larger than 10^5 because of the trend in the behavior of merging BICs [24]. The Q factors of single-resonance BICs and of quasi-BIC modes nearby are substantially larger than 10^6, that is, one order of magnitude larger than those in a very recent experimental demonstration of topologically enabled ultrahigh-Q quasi-BICs [24], indicating the possibility of an efficient way to guide diffraction-free beams beyond the light cone.

To evaluate the beam-guiding effect, we calculate the coupling of a Gaussian beam in free space to such a BIC mode by using the FEM, where perfectly matched layer boundary conditions are applied to absorb the outgoing wave. Because of limited computational power, we consider a finite PhC slab ($15a \times 40a$), which might introduce a Fabry-Perot cavity effect because of the abrupt variation of the permittivity. As can be seen from the evolution of the magnetic field [Re(H_z)] in Fig. 3(a), a Gaussian beam with a waist diameter of $4.7a$ preserves its width during propagation (over a length of $40a$, i.e.,$\sim$15.5λ, where λ is the wavelength), while the same beam suffers from significant diffraction in vacuum, as shown in Fig. 3(b) (see also Fig. S1 in the Supplemental Material [74]). More importantly, the out-of-plane scattering is cancelled by the single-resonance BIC. Both the tight confinement of the magnetic field shown in the upper panel of Fig. 3(c) and the flat phase front shown in the lower panel of Fig. 3(c) confirm the efficient out-of-plane beam guiding. As the two interfaces of the PhC slab are not optimized to reduce the impedance mismatch between the air and the PhC, the finite PhC slab behaves similarly to a Fabry-Perot cavity, as shown in Figs. 3(a) and 3(c). The coupling efficiency to the diffraction-free modes beyond the light cone

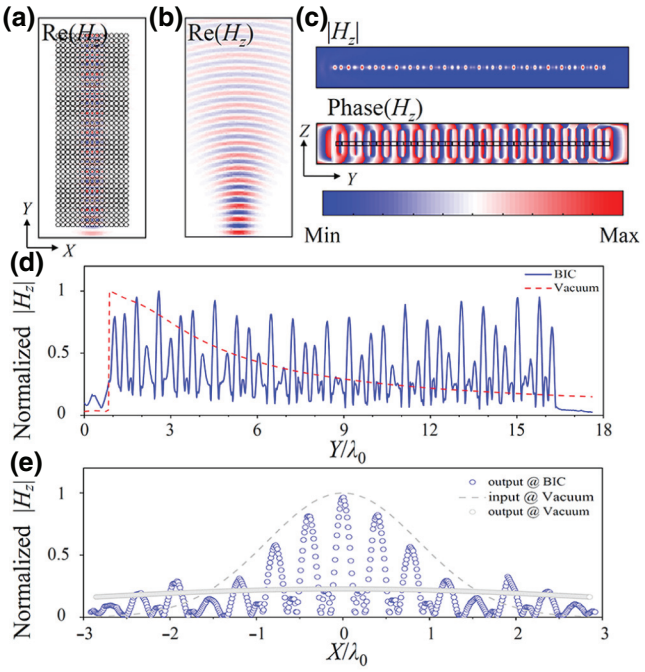

FIG. 3. (a),(b) Evolution of the magnetic field [Re(H_z)] in the X-Y plane when a Gaussian beam ($a/\lambda = 0.3885$ with a beam waist of $4.7a$) propagates in the proposed PhC slab with a size of $15a \times 40a$ unit cells (a) and in vacuum (b). (c) Evolution of magnetic field ($|H_z|$) and its corresponding phase distribution in the Y-Z plane shown in (a). (d) Normalized magnetic field amplitude ($|H_z|$) along the propagation direction under the BIC condition (blue line) and in vacuum (red line) at the same normalized frequency. (e) Normalized magnetic field amplitude of the input Gaussian beam (gray dashed line) and output beam (open circles) at the center of the PhC slab under the BIC condition (blue). The corresponding result for the output in vacuum (gray) is also shown.

can be optimized by engineering the shape of the interfaces or using waveguide couplers [10]. The cancellation of in-plane diffraction can be quantitatively evaluated by inspecting the amplitude of the magnetic field along the propagation direction, as shown in Fig. 3(d). Compared with the result for propagation in vacuum (dashed red line), the maximum amplitude of the SC mode beyond the light cone is almost unchanged during propagation (solid blue line). Furthermore, the input (dashed lines) and output (open circles) beam profiles shown in Fig. 3(e) also validate the in-plane diffraction-free and robust out-of-plane guiding nature of the BIC mode considered. The normalization of the output profile for the BIC case is performed utilizing the magnetic field after the input interface. The two cases are excited by the same Gaussian beam in vacuum. In order to prove that the SC mode is essentially beyond the light cone, we perform Fourier transformation of the magnetic field along the propagation direction shown in Fig. 3(a) and obtain a k vector of $0.795 \times 2\pi/a$, which is equal to that of the BIC mode at

the k value $0.205 \times 2\pi/a$ after taking the reciprocal lattice into account [see Fig. 2(c) for comparison]. Such on-chip diffraction-free beam quasiguiding beyond the light cone can be realized in a normalized frequency range $a/\lambda = 0.377$–0.389, as marked in Fig. 2(a) (see also Figs. S2 and S3 in the Supplemental Material [74]). More importantly, the proposed guiding mechanism is also compatible with an SC mode below the light cone, facilitating the dense integration and channelless multiplexing of polychromatic diffraction-free beams both beyond and below the light cone, as schematically shown in Fig. 1(a) (see also Fig. S4 in the Supplemental Material [74]).

III. MICROWAVE EXPERIMENTS

The underlying physics of the proposed diffraction-free beam-guiding mechanism is quite general and can be readily applied over a wide spectral range of electromagnetic waves. Here, we experimentally demonstrate the results using microwaves. The experimental setup used to measure the electromagnetic near field of the PhC slab is shown in Fig. 4(a).

A standard-gain horn antenna (HD-58SGAH20N) is connected to a vector network analyzer (VNA) (R&S ZNB40) to irradiate the slab with microwaves at frequencies from 4 to 7.5 GHz. A homemade loop antenna connected to the VNA is used as a magnetic field probe to measure the magnetic near field of the PhC slab, as indicated in Fig. 4(a). The loop antenna is mounted on a microwave scanning platform (LINBOU, NFS03 Floor Version) connected to the VNA, where the magnetic field can be acquired in a plane just above the slab. Microwave absorbers are used to minimize the impact of echo signals. Alumina ceramic disks ($\varepsilon = 9.6$, $15a \times 40a$, $a = 18.1$ mm) are used to construct the PhC slab, which is placed on a foam substrate ($\varepsilon \sim 1$), as shown in Fig. 4(a). We use an electromagnetic wave diffracted by a copper slot (of width $4.6a$) to mimic a Gaussian beam (H_z polarization) propagating along the Y axis, as indicated in the inset of Fig. 4(a). The measured S_{21} of the loop antenna, which is proportional to the magnetic field component [$\mathrm{Re}(S_{21})$, $f = 6.23$ GHz], and its corresponding phase distribution at the input and output regions marked in Fig. 4(a) are presented in Fig. 4(b) (see also Fig. S5 in the Supplemental

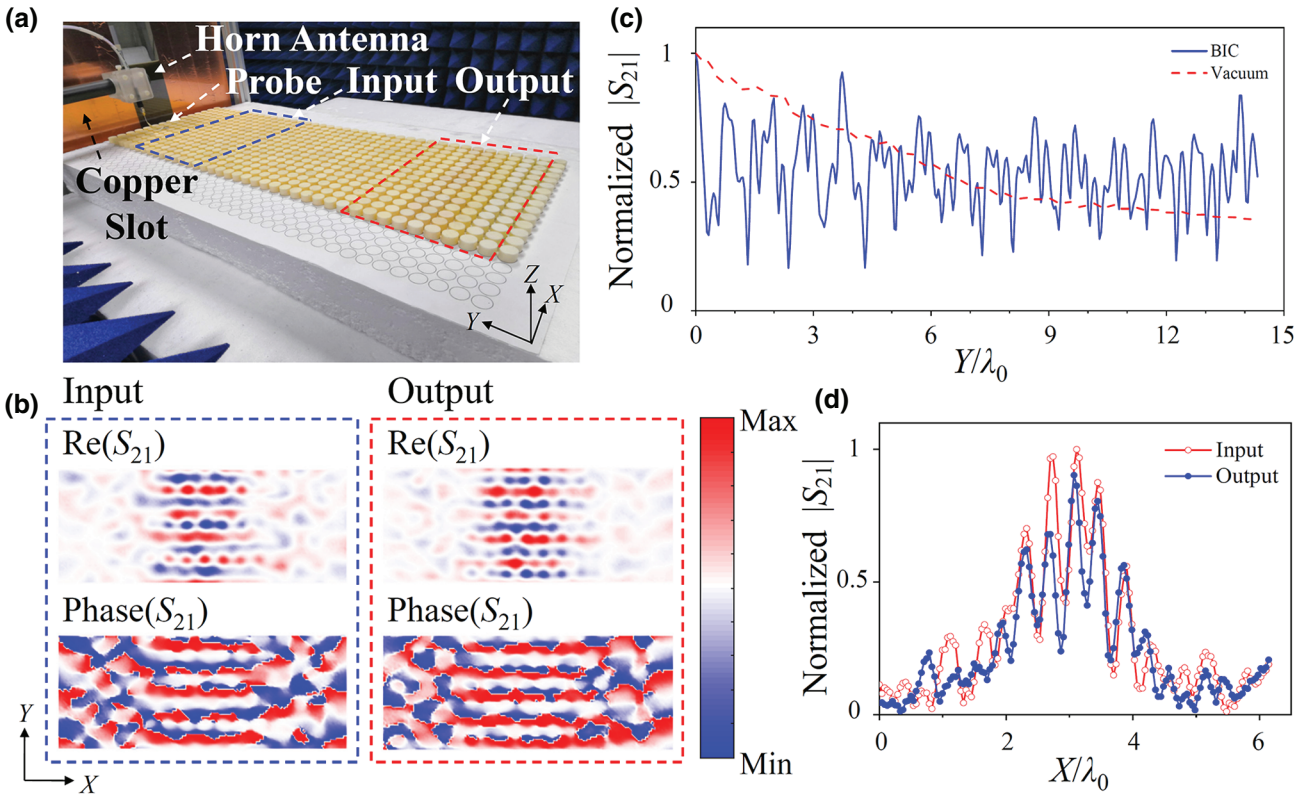

FIG. 4. (a) Experimental setup to measure the electromagnetic near-field distributions of the diffraction-free beam guiding beyond the light cone in a PhC slab with $15a \times 40a$ unit cells. The blue (red) dashed rectangle indicates the input (output) area measured in the experiment. (b) Experimental near-field mapping of $\mathrm{Re}(S_{21})$, proportional to the amplitude of the magnetic field at a frequency of 6.23 GHz, and corresponding phase distributions in the regions marked in (a). (c) Normalized $|S_{21}|$ along the propagation direction under the BIC condition (blue line) and in vacuum (red line) measured at the same frequency. (d) Input ($Y = 7a$) and output ($Y = 38a$) beam profiles.

Material [74]). As can be seen from these results, the beam size in the output region is similar to that in the input region, and both results share the same characteristic of a flat phase front. The evolution of the magnetic amplitude $|S_{21}|$ along the propagation direction in the PhC slab (solid blue line) and in vacuum (red dashed line) is shown in Fig. 4(c), while the input (open circles) and output (solid circles) magnetic field profiles measured above the PhC slab are plotted in Fig. 4(d). As can be seen from these results, the amplitude of the diffraction-free BIC mode is reduced very little in propagating over a distance of $40a$. We also perform Fourier transformation of the magnetic field ($a/\lambda = 0.376$) measured along the propagation direction, where an equivalent central k vector of $0.24 \times 2\pi/a$ is obtained. As a result, such modes are essentially beyond the light cone. The experimental results shown in Fig. 4 agree well with the numerical results shown in Fig. 3, which substantially validates the proposed diffraction-free beam guiding beyond the light cone. The small difference in the k vector obtained compared with the theoretical results is because of variation of the geometrical parameters. It should be also noted here that the electromagnetic wave diffracted from the copper slot has a more complex k-vector distribution, which in turn further strengthens the robustness of the proposed concept. In order to reduce the effects of the substrate, which could shift the targeted frequency for diffraction-free guiding, a membrane-based PhC slab could be a potential solution, which could be suspended to form a symmetrical system.

The diffraction-free beam propagation can be further validated by considering the scenario of excitation with a magnetic dipole. The experimental results under excitation with a loop antenna (mimicking the condition of excitation with a magnetic dipole) on top of a dielectric cylinder at the input facet are shown in Fig. 5. Compared with the simulation results for a magnetic dipole in vacuum, the unexpanded beam width and the flat wave fronts in the measured distributions of the real part, phase, and amplitude of S_{21} consolidate the evidence for a diffraction-free beam-guiding effect beyond the light cone. According to the result of Fourier transforming the magnetic field, the central k vector obtained is $0.2467 \times 2\pi/a$, which indicates that this guiding effect is indeed beyond the light cone.

One of the interesting properties of quasi-BICs is that they can facilitate the coupling of excitations in the continuum to quasiguided modes. In order to validate the possibility of external coupling to diffraction-free beam guiding beyond the light cone, we calculate the coupling of an inclined (at 30°) Gaussian beam with the same width

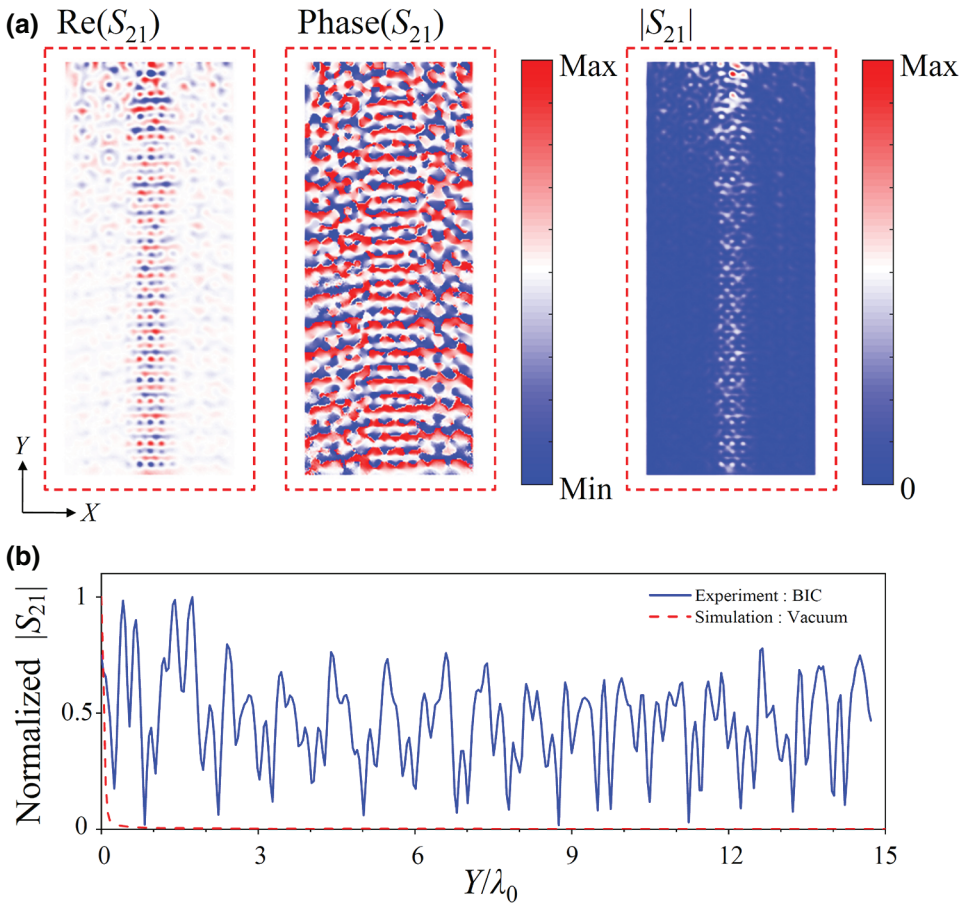

FIG. 5. (a) Experimental near-field mapping of Re(S_{21}), the corresponding phase of S_{21}, and $|S_{21}|$ for the structure shown in Fig. 4(a) at a frequency of 6.22 GHz. The area measured is above the whole PhC structure. (b) Normalized magnetic field amplitude ($|S_{21}|$) along the propagation direction under the quasi-BIC condition, measured at the same frequency (blue solid line); the corresponding simulation result in vacuum is shown by the red dashed line.

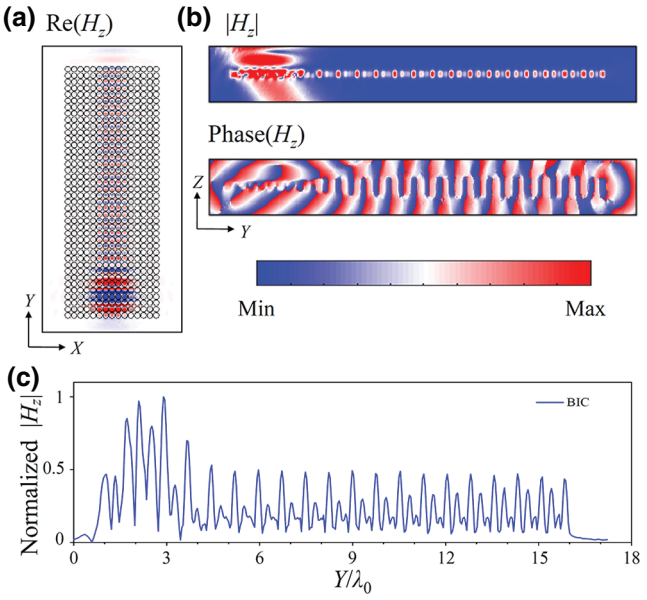

FIG. 6. Coupling of an inclined Gaussian beam (at 30°) to a diffraction-free beam beyond the light cone. The width of the Gaussian beam is similar to that in Fig. 3(a). Distributions of Re(H_z) on the X-Y plane just above the PhC slab (a) and $|H_z|$ on the mirror Y-Z plane (b). The corresponding phase distribution is also presented in (b). (c) Evolution of normalized $|H_z|$ along the propagation direction at the center of the beam.

as that in Fig. 3 to the diffraction-free modes; the results are shown in Fig. 6. As can be seen from these figures, the flat wave fronts shown in Figs. 6(a) and 6(b), as well as the evolution of the magnetic field amplitude along the propagation direction, validate that the channelless diffraction-free beam guiding beyond the light cone can be accessed by inclined excitation, which might find potential applications in integrated optics. The coupling efficiency might be improved by use of the recently suggested unidirectional BICs [62].

IV. DISCUSSION AND CONCLUSION

In summary, we propose a physical mechanism to realize on-chip diffraction-free beam guiding beyond total internal reflection. Out-of-plane scattering is prohibited by the physics of BICs, while in-plane diffraction is cancelled by the tailored spatial dispersion of the PhC slab. Microwave experiments further support the theoretical proposal. The operation-frequency and k-vector ranges might be enlarged by applying the recently proposed merging BICs near the SC mode [24], which simultaneously increase the robustness to fabrication disorder. The on-chip diffraction-free beam guiding beyond the light cone not only facilitates a wide variety of applications, including but not limited to free-space coupling to the channelless SC quasiguided modes, mode sorting, beam routing, sensing, and lasing, but also, more importantly, opens up an avenue for exploring guided-wave physics beyond the light cone. Furthermore, it can shed light on the wave-guiding mechanism in various wave-physics systems, such as in acoustics [75] and non-Hermitian physics [76].

ACKNOWLEDGMENTS

Y. Xu thanks Dr. Menglin L. N. Chen for her suggestions for the microwave experiments. This research was supported by the National Natural Science Foundation of China (NSFC) (Grants No. 91750110, No. 11674130, No. 11704156, No. 11674110, No. 11874437, and No. 11874020), the Natural Science Foundation of Guangdong Province, China (Grants No. 2016A030306016, No. 2016TQ03X981, and No. 2016A030308010), and the Pearl River Nova Program of Guangzhou (Grant No. 201806010040).

[1] A. W. Snyder and J. D. Love, *Optical Waveguide Theory* (Springer Science & Business Media, New York, 2012).
[2] M. Noori, M. Soroosh, and H. Baghban, Self-collimation in photonic crystals: Applications and opportunities, Ann. Phys. **530**, 1700049 (2017).
[3] D. N. Christodoulides, F. Lederer, and Y. Silberberg, Discretizing light behaviour in linear and nonlinear waveguide lattices, Nature (London) **424**, 817 (2003).
[4] Z. Chen, M. Segev, and D. N. Christodoulides, Optical spatial solitons: Historical overview and recent advances, Rep. Prog. Phys. **75**, 086401 (2012).
[5] I. L. Garanovich, S. Longhi, A. A. Sukhorukov, and Y. S. Kivshar, Light propagation and localization in modulated photonic lattices and waveguides, Phys. Rep. **518**, 1 (2012).
[6] H. Kosaka, T. Kawashima, A. Tomita, M. Notomi, T. Tamamura, T. Sato, and S. Kawakami, Self-collimating phenomena in photonic crystals, Appl. Phys. Lett. **74**, 1212 (1999).
[7] H. S. Eisenberg, Y. Silberberg, R. Morandotti, and J. S. Aitchison, Diffraction Management, Phys. Rev. Lett. **85**, 1863 (2000).
[8] T. Pertsch, T. Zentgraf, U. Peschel, A. Bräuer, and F. Lederer, Anomalous Refraction and Diffraction in Discrete Optical Systems, Phys. Rev. Lett. **88**, 093901 (2002).
[9] J. Witzens, M. Loncar, and A. Scherer, Self-collimation in planar photonic crystals, IEEE J. Sel. Top. Quantum Electron. **8**, 1246 (2002).
[10] L. Wu, M. Mazilu, and T. F. Krauss, Beam steering in planar-photonic crystals: From superprism to supercollimator, J. Lightwave Technol. **21**, 561 (2003).
[11] D. W. Prather, S. Shi, D. M. Pustai, C. Chen, S. Venkataraman, A. Sharkawy, G. J. Schneider, and J. Murakowski, Dispersion-based optical routing in photonic crystals, Opt. Lett. **29**, 50 (2004).
[12] D. N. Chigrin, S. Enoch, C. M. S. Torres, and G. Tayeb, Self-guiding in two-dimensional photonic crystals, Opt. Express **11**, 1203 (2003).
[13] P. T. Rakich, M. S. Dahlem, S. Tandon, M. Ibanescu, M. Soljačić, G. S. Petrich, J. D. Joannopoulos, L. A.

Kolodziejski, and E. P. Ippen, Achieving centimetre-scale supercollimation in a large-area two-dimensional photonic crystal, Nat. Mater. **5**, 93-96 (2006).

[14] Y. Xu, X. J. Chen, S. Lan, Q. Guo, W. Hu, and L. J. Wu, The all-angle self-collimating phenomenon in photonic crystals with rectangular symmetry, J. Opt. A: Pure Appl. Opt. **10**, 085201 (2008).

[15] V. Mocella, S. Cabrini, A. S. P. Chang, P. Dardano, L. Moretti, I. Rendina, D. Olynick, B. Harteneck, and S. Dhuey, Self-Collimation of Light Over Millimeter-Scale Distance in a Quasi-Zero-Average-Index Metamaterial, Phys. Rev. Lett. **102**, 133902 (2009).

[16] S. Kocaman, R. Chatterjee, N. C. Panoiu, J. F. McMillan, M. B. Yu, R. M. Osgood, D. L. Kwong, and C. W. Wong, Observation of Zeroth-Order Band Gaps in Negative-Refraction Photonic Crystal Superlattices at Near-Infrared Frequencies, Phys. Rev. Lett. **102**, 203905 (2009).

[17] L. Gan, F. Qin, and Z. Y. Li, Broadband large-angle self-collimation in two-dimensional silicon photonic crystal, Opt. Lett. **37**, 2412 (2012).

[18] J. Arlandis, E. Centeno, R. Pollès, A. Moreau, J. Campos, O. Gauthier-Lafaye, and A. Monmayrant, Mesoscopic Self-Collimation and Slow Light in All-Positive Index Layered Photonic Crystals, Phys. Rev. Lett. **108**, 037401 (2012).

[19] H. Li, A. Wu, W. Li, X. Lin, C. Qiu, Z. Sheng, X. Wang, S. Zou, and F. Gan, Millimeter-scale and large-angle self-collimation in a photonic crystal composed of silicon nanorods, IEEE Photon. J. **5**, 2201306 (2013).

[20] G. Ru, Y. Zheng, J. Liu, and X. Jiang, Hyper collimation ability of two-dimensional photonic crystals, Opt. Express **27**, 11968 (2019).

[21] R. A. Vicencio, C. Cantillano, L. Morales-Inostroza, B. Real, C. Mejía-Cortés, S. Weimann, A. Szameit, and M. I. Molina, Observation of Localized States in Lieb Photonic Lattices, Phys. Rev. Lett. **114**, 245503 (2015).

[22] J. v. Neumann and E. Wigner, übermerkwüdigediskreteEigenwerte, Phys. Z. **30**, 465 (1929).

[23] H. Friedrich and D. Wintgen, Physical realization of bound states in the continuum, Phys. Rev. A **31**, 3964 (1985).

[24] J. Jin, X. Yin, L. Ni, M. Soljačić, B. Zhen, and C. Peng, Topologically enabled ultra-high-Q guided resonances robust to out-of-plane scattering, Nature **574**, 501 (2019).

[25] E. N. Bulgakov and D. N. Maksimov, Topological Bound States in the Continuum in Arrays of Dielectric Spheres, Phys. Rev. Lett. **118**, 267401 (2017).

[26] T. C. Lim and G. W. Farnell, Character of pseudo surface waves on anisotropic crystals, J. Acoust. Soc. Am. **45**, 845 (1969).

[27] F. Capasso, C. Sirtori, J. Faist, D. L. Sivco, S. N. G. Chu, and A. Y. Cho, Observation of an electronic bound state above a potential well, Nature (London) **358**, 565 (1992).

[28] P. J. Cobelli, V. Pagneux, A. Maurel, and P. Petitjeans, Experimental observation of trapped modes in a water wave channel, Europhys. Lett. **88**, 20006 (2009).

[29] R. F. Ndangali and S. V. Shabanov, Electromagnetic bound states in the radiation continuum for periodic double arrays of subwavelength dielectric cylinders, J. Math. Phys. **51**, 102901 (2010).

[30] C. W. Hsu, B. Zhen, A. D. Stone, J. D. Joannopoulos, and M. Soljačić, Bound states in the continuum, Nat. Rev. Mater. **1**, 16048 (2016).

[31] S. Fan and J. D. Joannopoulos, Analysis of guided resonances in photonic crystal slabs, Phys. Rev. B **65**, 235112 (2002).

[32] E. N. Bulgakov and A. F. Sadreev, Bound states in the continuum in photonic waveguides inspired by defects, Phys. Rev. B **78**, 075105 (2008).

[33] Y. Plotnik, O. Peleg, F. Dreisow, M. Heinrich, S. Nolte, A. Szameit, and M. Segev, Experimental Observation of Optical Bound States in the Continuum, Phys. Rev. Lett. **107**, 183901 (2011).

[34] S. Weimann, Y. Xu, R. Keil, A. E. Miroshnichenko, A. Tünnermann, S. Nolte, A. A. Sukhorukov, A. Szameit, and Y. S. Kivshar, Compact Surface Fano States Embedded in the Continuum of Waveguide Arrays, Phys. Rev. Lett. **111**, 240403 (2013).

[35] M. I. Molina, A. E. Miroshnichenko, and Y. S. Kivshar, Surface Bound States in the Continuum, Phys. Rev. Lett. **108**, 070401 (2012).

[36] J. Lee, B. Zhen, S.-L. Chua, W. Qiu, J. D. Joannopoulos, M. Soljačić, and O. Shapira, Observation and Differentiation of Unique High-Q Optical Resonances near Zero Wave Vector in Macroscopic Photonic Crystal Slabs, Phys. Rev. Lett. **109**, 067401 (2012).

[37] C. W. Hsu, B. Zhen, J. Lee, S. L. Chua, S. G. Johnson, J. D. Joannopoulos, and M. Soljačić, Observation of trapped light within the radiation continuum, Nature **499**, 188 (2013).

[38] C. W. Hsu, B. Zhen, S.-L. Chua, S. G. Johnson, J. D. Joannopoulos, and M. Soljačić, Bloch surface eigenstates within the radiation continuum, Light Sci. Appl. **2**, e84 (2013).

[39] Y. Yang, C. Peng, and Z. Li, Semi-analytical approach for guided mode resonance in high-index-contrast photonic crystal slab: TE polarization, Opt. Express **21**, 20588 (2013).

[40] F. Monticone and A. Alù, Embedded Photonic Eigenvalues in 3D Nanostructures, Phys. Rev. Lett. **112**, 213903 (2014).

[41] Y. Yang, C. Peng, Y. Liang, Z. Li, and S. Noda, Analytical Perspective for Bound States in the Continuum in Photonic Crystal Slabs, Phys. Rev. Lett. **113**, 037401 (2014).

[42] B. Zhen, C. W. Hsu, L. Lu, A. D. Stone, and M. Soljačić, Topological Nature of Optical Bound States in the Continuum, Phys. Rev. Lett. **113**, 257401 (2014).

[43] A. Kodigala, T. Lepetit, Q. Gu, B. Bahari, Y. Fainman, and B. Kanté, Lasing action from photonic bound states in continuum, Nature (London) **541**, 196 (2017).

[44] J. Gomis-Bresco, D. Artigas, and L. Torner, Anisotropy-induced photonic bound states in the continuum, Nat. Photonics **11**, 232 (2017).

[45] Y. Guo, M. Xiao, and S. Fan, Topologically Protected Complete Polarization Conversion, Phys. Rev. Lett. **119**, 167401 (2017).

[46] M. V. Rybin, K. L. Koshelev, Z. F. Sadrieva, K. B. Samusev, A. A. Bogdanov, M. F. Limonov, and Y. S. Kivshar, High-Q Supercavity Modes in Subwavelength Dielectric Resonators, Phys. Rev. Lett. **119**, 243901 (2017).

[47] K. Koshelev, S. Lepeshov, M. Liu, A. Bogdanov, and Y. Kivshar, Asymmetric Metasurfaces with High-Q

Resonances Governed by Bound States in the Continuum, Phys. Rev. Lett. **121**, 193903 (2018).

[48] Z. F. Sadrieva, I. S. Sinev, K. L. Koshelev, A. Samusev, I. V. Iorsh, O. Takayama, R. Malureanu, A. A. Bogdanov, and A. V. Lavrinenko, Transition from optical bound states in the continuum to leaky resonances: Role of substrate and roughness, ACS Photonics **4**, 723 (2017).

[49] S. T. Ha, Y. H. Fu, N. K. Emani, Z. Pan, R. M. Bakker, R. Paniagua-Domínguez, and A. I. Kuznetsov, Directional lasing in resonant semiconductor nanoantenna arrays, Nat. Nanotechnol. **13**, 1042 (2018).

[50] A. Tittl, A. Leitis, M. Liu, F. Yesilkoy, D. Y. Choi, D. N. Neshev, Y. S. Kivshar, and H. Altug, Imaging-based molecular barcoding with pixelated dielectric metasurfaces, Science **360**, 1105 (2018).

[51] Y. Zhang, A. Chen, W. Z. Liu, C. W. Hsu, B. Wang, F. Guan, X. H. Liu, L. Shi, L. Lu, and J. Zi, Observation of Polarization Vortices in Momentum Space, Phys. Rev. Lett. **120**, 186103 (2018).

[52] H. M. Doeleman, F. Monticone, W. den Hollander, A. Alù, and A. F. Koenderink, Experimental observation of a polarization vortex at an optical bound state in the continuum, Nat. Photonics **12**, 397 (2018).

[53] S. Dai, L. Liu, D. Han, and J. Zi, From topologically protected coherent perfect reflection to bound states in the continuum, Phys. Rev. B **98**, 081405(R) (2018).

[54] Y. He, G. T. Guo, T. H. Feng, Y. Xu, and A. E. Miroshnichenko, Toroidal dipole bound states in the continuum, Phys. Rev. B **98**, 161112(R) (2018).

[55] M. Minkov, I. A. D. Williamson, M. Xiao, and S. Fan, Zero-Index Bound States in the Continuum, Phys. Rev. Lett. **121**, 263901 (2018).

[56] S. I. Azzam, V. M. Shalaev, A. Boltasseva, and A. V. Kildishev, Formation of Bound States in the Continuum in Hybrid Plasmonic-Photonic Systems, Phys. Rev. Lett. **121**, 253901 (2018).

[57] M. Liu and D.-Y. Choi, Extreme Huygens' metasurfaces based on quasi-bound states in the continuum, Nano Lett. **18**, 8062 (2018).

[58] F. Yesilkoy, E. R. Arvelo, Y. Jahani, M. Liu, A. Tittl, V. Cevher, Y. Kivshar, and H. Altug, Ultrasensitive hyperspectral imaging and biodetection enabled by dielectric metasurfaces, Nat. Photonics **13**, 390 (2019).

[59] W. Liu, B. Wang, Y. Zhang, J. Wang, M. Zhao, F. Guan, X. Liu, L. Shi, and J. Zi, Circularly Polarized States Spawning from Bound States in the Continuum, Phys. Rev. Lett. **123**, 116104 (2019).

[60] A. S. Kupriianov, Y. Xu, A. Sayanskiy, V. Dmitriev, Y. S. Kivshar, and V. R. Tuz, Metasurface Engineering through Bound States in the Continuum, Phys. Rev. Appl. **12**, 014024 (2019).

[61] Z. Liu, Y. Xu, Y. Lin, J. Xiang, T. Feng, Q. Cao, J. Li, S. Lan, and J. Liu, High-Q Quasibound States in the Continuum for Nonlinear Metasurfaces, Phys. Rev. Lett. **123**, 253901 (2019).

[62] X. Yin, J. Jin, M. Soljačić, C. Peng, and B. Zhen, Observation of unidirectional bound states in the continuum enabled by topological defects, Nature **580**, 467 (2020).

[63] C. L. Zou, J. M. Cui, F. W. Sun, X. Xiong, X. B. Zou, Z. F. Han, and G. C. Guo, Guiding light through optical bound states in the continuum for ultrahigh-Q microresonators, Laser Photon. Rev. **9**, 114 (2015).

[64] E. N. Bulgakov and D. N. Maksimov, Light guiding above the light line in arrays of dielectric nanospheres, Opt. Lett. **41**, 3888 (2016).

[65] Z. Hu and Y. Y. Lu, Propagating bound states in the continuum at the surface of a photonic crystal, J. Opt. Soc. Am. B **34**, 1878 (2017).

[66] E. N. Bulgakov and A. F. Sadreev, Propagating Bloch bound states with orbital angular momentum above the light line in the array of dielectric spheres, J. Opt. Soc. Am. A **34**, 949 (2017).

[67] E. Bulgakov and A. Sadreev, Fibers based on propagating bound states in the continuum, Phys. Rev. B **98**, 085301 (2018).

[68] E. N. Bulgakov, D. N. Maksimov, P. N. Semina, and S. A. Skorobogatov, Propagating bound states in the continuum in dielectric gratings, J. Opt. Soc. Am. B **35**, 1218 (2018).

[69] Z. Yu, X. Xi, J. Ma, H. K. Tsang, C.-L. Zou, and X. Sun, Photonic integrated circuits with bound states in the continuum, Optica **6**, 1342 (2019).

[70] L. Ni, Z. Wang, C. Peng, and Z. Li, Tunable optical bound states in the continuum beyond in-plane symmetry protection, Phys. Rev. B **94**, 245148 (2016).

[71] X. Gao, C. W. Hsu, B. Zhen, X. Lin, J. D. Joannopoulos, M. Soljačić, and H. Chen, Formation mechanism of guided resonances and bound states in the continuum in photonic crystal slabs, Sci. Rep. **6**, 31908 (2016).

[72] Z. Dai, Y. Xu, Q. Guo, and S. Chi, Beam propagation in two-dimensional media with spatial dispersion, Phys. Rev. A **87**, 053827 (2013).

[73] P. Kaspar, R. Kappeler, D. Erni, and H. Jäckel, Relevance of the light line in planar photonic crystal waveguides with weak vertical confinement, Opt. Express **19**, 24344 (2011).

[74] See Supplemental Material at http://link.aps.org/supplemental/10.1103/PhysRevApplied.13.064032 for the evolution of Gaussian beams propagating in the PhC slab, multiplexing of diffraction-free beam guiding beyond and below the light cone, and experimental results on diffraction-free beam guiding beyond the light cone.

[75] H. Yang, X. Zhang, D. Zhao, Y. Liu, J. Guo, Y. Yao, and F. Wu, The self-collimation effect induced by non-Hermitian acoustic systems, Appl. Phys. Lett. **114**, 133503 (2019).

[76] W. W. Ahmed, R. Herrero, M. Botey, and K. Staliunas, Self-collimation in PT-symmetric crystals, Phys. Rev. A **95**, 053830 (2017).